


Massive particle acceleration on a photonic chip via spatial-temporal modulation

Mai Zhang,^{1,2,†} Xie-Hang Yu^{1,2,†}, Xin-Biao Xu,^{1,2} Guang-Can Guo,^{1,2} and Chang-Ling Zou^{1,2,*}

¹*CAS Key Laboratory of Quantum Information, University of Science and Technology of China, Hefei, Anhui 230026, People's Republic of China*

²*CAS Center For Excellence in Quantum Information and Quantum Physics, University of Science and Technology of China, Hefei, Anhui 230026, People's Republic of China*

 (Received 17 April 2022; revised 31 May 2023; accepted 25 October 2023; published 21 November 2023)

Recently, the spectral manipulation of single photons has been achieved through spatial-temporal modulation of the optical refractive index. Here, we utilized the spatial-temporal modulation of the potential to manipulate the motion of massive particles, i.e., realizing the MeV-magnitude electron acceleration and atom decelerator on a millimeter scale. With the language of spatial-temporal modulation, manipulation of the photons and massive particles are connected and clearly investigated. The spatial-temporal modulation approach is also powerful for the optimization of multistage modulation with a large number of single stages on a photonic integrated chip and can be generalized to a wide range of systems. Thus, this approach may play a significant role in hybrid photonic chips and microscale particle manipulation.

DOI: [10.1103/PhysRevApplied.20.054045](https://doi.org/10.1103/PhysRevApplied.20.054045)

I. INTRODUCTION

The photonic chip offers a united platform to investigate and utilize light-matter interactions. This compact, stable, and scalable platform allows the integration of thousands of functional photonic devices on a single chip [1–7]. Of note, the light-matter interaction could be greatly enhanced on the chip, due to the strong confinement of optical fields in photonic microstructures with a nanoscale cross section [8–13] and the resonant enhancement [14–16] in microcavities. Benefiting from these advantages of photonic chips, manipulation of optical photons has recently been realized in tens of distributed optomechanical waveguides [17]. It was demonstrated that when certain spatial-temporal modulation is applied to optical photons, their spectral features could be manipulated with very high efficiency.

On a photonic chip, the motion of massive particles could also be manipulated through the optical field. For instance, the optical dipole force could be applied to trap and transport nanoparticles or atoms [18–24]. Recently, optical fields in photonic microstructures have been applied to manipulate free electrons [13,25–31], which provide alternative tools to investigate and control both photons and electrons [32–38]. It is anticipated that the approach of distributed spatial-temporal modulation could be helpful for improving the efficiency of the massive particle manipulation. For the manipulation of photons, the interaction could accumulate with the propagation of photons when the phase-matching condition of

the nonlinear optics effect is satisfied for a given device and working wavelength [39]. However, for the manipulation of massive particles, the coupling between the massive particle and optical fields varies with the propagation of the particle as its velocity changes [40]. Therefore, the investigation of the corresponding phase-matching condition is crucial for manipulating massive particles by distributed spatial-temporal modulations.

In this paper, we generalize the theory of spatial-temporal modulation to the interaction between massive particles and space-time varying potential. With the generalized theory of spatial-temporal modulation, concepts in different systems, i.e., phase-matching condition for nonlinear optics and the synchronicity condition for accelerator physics, are connected and a spatial-temporal matching (STM) condition is derived for massive particles. The distributed spatial-temporal modulation approach to achieve STM conditions is especially efficient for the design of cascaded electron accelerators with a large number of single stages. It is demonstrated that a portion of 10% electrons in an initially Gaussian distributed ensemble can be accelerated by 200 keV within a length less than 6 mm.

II. PRINCIPLE OF SPATIAL-TEMPORAL MODULATION

First, we explain the general theory of spatial-temporal modulation by experimentally verified optical frequency manipulation on a photonic chip [41], where photons travel in a waveguide while there are distributed mechanical vibrations changing the effective refractive index of the

*clzou321@ustc.edu.cn

†These two authors contributed equally to this work.

waveguide as $\Delta n_{\text{eff}}(x, t)$. The photon energy is adiabatically shifted as (Appendix B):

$$\delta E \approx \hbar v_g k_0 \int d\zeta \frac{\partial}{\partial x} [\Delta n_{\text{eff}}(x, t)], \quad (1)$$

which is integrated along its trajectory ζ . Here, \hbar is the reduced Planck constant, v_g is the optical group velocity in the waveguide, and k_0 is the vacuum photon wave vector. Introducing the spatial-temporal potential $U(x, t) = -v_g \hbar k_0 \Delta n_{\text{eff}}(x, t)$, the manipulation of photon self-energy can be written in a general form as

$$\delta E = - \int \frac{\partial U(x, t)}{\partial x} d\zeta. \quad (2)$$

This expression works for both massless and massive particles to describe the change in the traveling particle's self-energy by a spatial-temporal potential. For massless particles, such as photons, self-energy manipulation corresponds to the frequency shift, while for massive particles, such as electrons and atoms, self-energy manipulation corresponds to acceleration or deceleration.

Figure 1(a) illustrates the interaction between particles and a typical harmonically modulating potential $U(x, t) = A \cos(\omega t - kx + \phi_0)$, with A , ω , k , and ϕ_0 denoting the amplitude, angular frequency, wave vector, and initial phase of the modulation, respectively. In a single modulation unit of length L with uniform A and k , the self-energy change can be approximated to the first order, i.e., the change in the particle velocity within the unit is negligible, as

$$\begin{aligned} \delta E(L) = & -\frac{2Akv_0}{\omega - kv_0} \sin \left[\frac{\omega L}{2v_0} - \frac{kL}{2} + \phi_0 \right] \\ & \times \sin \left[\frac{\omega L}{2v_0} - \frac{kL}{2} \right]. \end{aligned} \quad (3)$$

Therefore, the spatial-temporal matching condition is fulfilled when $\phi_0 = 3\pi/2$ and $\omega - kv_0 = 0$, in which case the particles experience a constant and maximum force and the corresponding energy gain can reach the optimal value $\delta E = AkL$. When $k = \omega/v$, as indicated by the yellow dot in Fig. 1(a), the particle's position with respect to the potential profile remains unchanged at different times. If $\phi_0 = 3\pi/2$ is satisfied initially, the particle will stay at the position where the gradient of the potential is maximum. As the change in the particle velocity is negligible, the STM is maintained when cascading the same units to enlarge L . This corresponds to the phase-matching condition in optics, under which the frequency shift increases with the interaction length (Appendix C).

However, the change in a particle's velocity is not negligible for a large L . Three examples of spatial-temporal modulation, where a particle's trajectory (green line) and

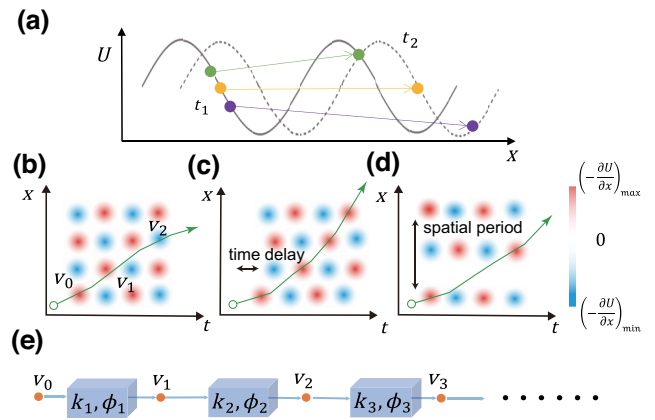


FIG. 1. (a) The evolution of particles in potential U for particle velocity v equal to, slower than, and faster than the group velocity of the spatial-temporal modulation of the potential. (b)–(d) Sketches of the spatial-temporal modulation process in the $x-t$ plot. The green lines show the trajectories of a particle, whose velocity increases when passing through the acceleration (red) area and decreases when passing through the deceleration (blue) area. (e) The general setup for massive particle manipulation via cascaded spatial-temporal modulation units, with k_i and ϕ_i representing the wave vector and phase parameters of the i th unit and v_i representing the velocity of the particle exiting from the i th unit.

the corresponding velocity change are considered, are schematically illustrated in Figs. 1(b)–1(d). The red and blue areas show the acceleration and deceleration zones for a given time and location (t and x). According to Fig. 1(a), the color of areas alternately changes along the x or t axis for harmonic modulation, as shown in Fig. 1(b). For such a periodic distribution, the STM condition will eventually be broken due to the change in the particle's velocity. By regulating the time delay in different locations [Fig. 1(c)] or the spatial period [Fig. 1(d)] of the modulation, a global STM in which the trajectory for a given particle's initial parameter only passes through acceleration zones can be achieved. However, this continuously varying field is experimentally challenging, and we resorted to the approach that divides the potential into multiple units, as shown in Fig. 1(e). The spatial period, i.e., the wave vector k_i is adjusted to match the velocity of the particle, and the time delay, i.e., the phase ϕ_i is introduced to maintain matching between different units. Thus, the global STM could be achieved in such a multiunit system. The global STM is also known as the Wideroes synchronicity condition in accelerator physics, which has been demonstrated in cascaded traveling-wave linear accelerators [42,43] with different structure periods.

The cascaded structures are flexible for an integrated photonic chip, as demonstrated in Ref. [17] where the photon frequency modulation is greatly enhanced. Benefiting

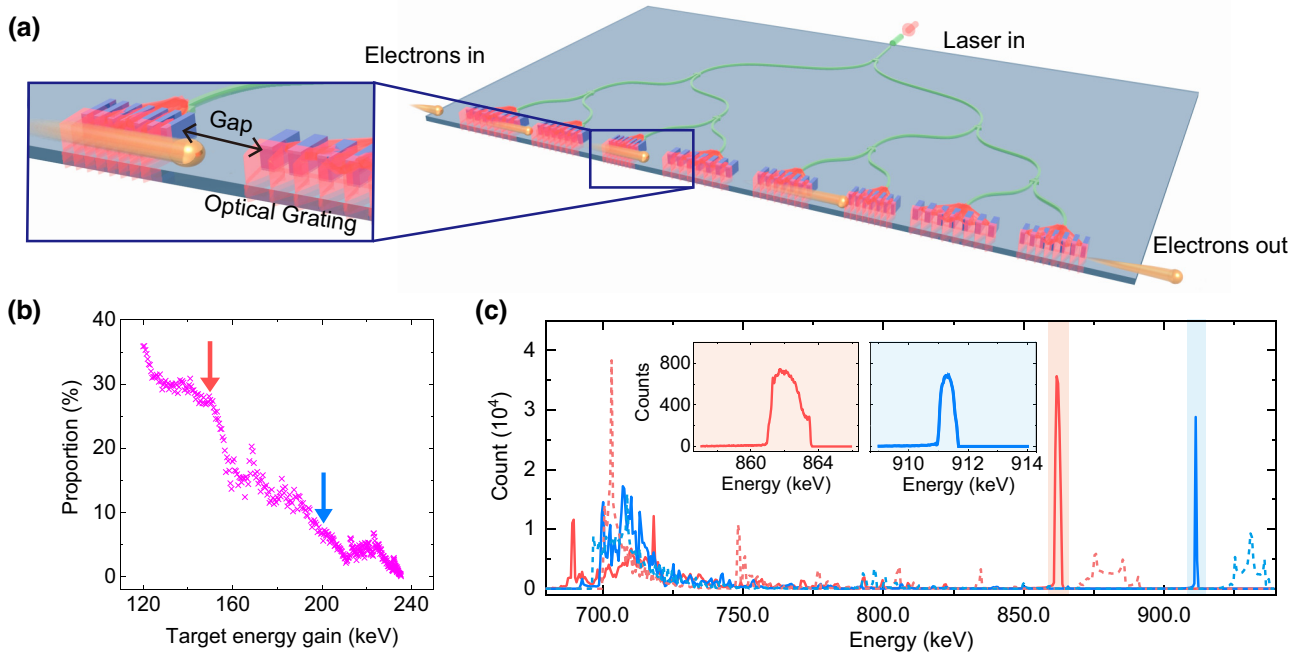


FIG. 2. (a) Sketch of the experimental setup for cascaded electron accelerator on a photonic chip. (b) The results of the proportion that the electron could gain energy that exceeds the target (horizontal axis), with the parameters of all units are optimized numerically and the initial energy distribution of the electron ensembles is set as a Gaussian function with a center at 711 keV with a standard deviation of 0.14 keV and the initial phase is random. The electrical field strength is 5×10^8 V/m, the unit length is 5.21 μm . (c) The final distribution of 500-k input electrons for different target energy gain, here the energy interval is 0.5 keV. The red line shows the result when the target energy gain is 150 keV, and the blue line shows the 200-keV situation. Dashed lines show the results for the parameters from the synchronicity condition. Inset: distribution around two peaks, here the energy interval is 10 eV.

from the advanced design and fabrication of photonic devices [1–7], even an arbitrary spatial-temporal potential field $U(x, t)$ can be realized by photonic chips. Additionally, the size of photonic devices could be significantly reduced, and the optical fields can be strongly concentrated on a chip. Since the mechanism of spatial-temporal modulation of photons can be generalized to massive particles traveling in the potential field, the photonic chip offers an excellent platform for the precise manipulation of massive particles. For example, optical potential fields under STM conditions on a photonic chip would benefit electron accelerators by utilizing the electric potential, atom slower through the ac Stark potential imposed by nanostructured optical fields, nanoparticle trapping through optical and acoustic tweezers, and so on. More details about the atom slower and the comparison between the massive and massless particle manipulation are provided in Appendix A. In the following, we focus on the investigation of the on-chip multistage linear accelerator of electrons.

III. ELECTRON ACCELERATOR

Figure 2(a) sketches the integrated grating structures for electron acceleration. Each section of the grating provides the evanescent electromagnetic field when illuminated by

a laser beam, which was experimentally studied in Ref. [25,26]. The oscillation frequency of the electric field ω is determined by the input laser, and the wave vector of the corresponding potential (k) is controllable by choosing an appropriate grating period. Hence, the STM could be realized when the electron and the spatial-temporal modulation field evolve at the same velocity as $v = \omega/k$. Meanwhile, the phase ϕ_0 can be directly controlled by an optical delay or the gap length between gratings. Therefore, the photonic chip provides a flexible platform to integrate hundreds of units that satisfy the STM condition for considerable electron acceleration on a cm-scale chip [Fig. 2(a)].

According to Eq. (2), the kinetic energy change of the electron in each unit is $\delta E = -e\mathcal{E}v \int_{t_0}^{t_0+\delta t} \sin(\omega t - kv t + \phi_0) dt$ to the first-order approximation, with \mathcal{E} being the amplitude of the induced evanescent field. To determine the parameters of each unit for the STM, the recurrence relation of the energy and phase distribution of an electron ensemble between two adjacent units can be analytically derived. For an input electron ensemble, with $f_n(E_n, \phi_n)$ represents the distribution of the energy and phase of the electrons entering the $(n+1)$ th unit, where E_n and ϕ_n are the corresponding energy and phase, respectively. The mapping between inputs at the $(n+1)$ th and $(n+2)$ th units is described by $E_{n+1} = E_n +$

δE , $\phi_{n+1} = \phi_n + (L/v)\omega + \Delta\phi_{n,n+1}$, where $\Delta\phi_{n,n+1}$ is the controllable phase difference. Therefore, the evolution of the distribution follows

$$f_{n+1}(E_{n+1}, \phi_{n+1}) = \left| \frac{\partial(E_n, \phi_n)}{\partial(E_{n+1}, \phi_{n+1})} \right| f_n(E_n, \phi_n). \quad (4)$$

However, sometimes we are more interested in the distribution of energy gain during the n th accelerator, which we will denote as $g_n(\Delta E_n)$. Here ΔE_n is defined with respect to the mean energy of the electron ensemble

$$\bar{E} = \int E_{n-1} f_{n-1}(E_{n-1}, \phi_{n-1}) d\phi_{n-1} dE_{n-1}. \quad (5)$$

Therefore, g_n can be calculated through f_{n-1} by

$$g_n(\Delta E_n) = \int_{\text{contour}} ds \frac{f_{n-1}(E_{n-1}, \phi_{n-1})}{|\nabla(\Delta E_n)|}. \quad (6)$$

The integral is calculated along the contour with respect to $\Delta E_n(E_{n-1}, \phi_{n-1})$ in the $\{E_{n-1}, \phi_{n-1}\}$ phase space. For the first accelerator unit, the time electrons arrive at the accelerator is usually uncontrollable compared to the period of the oscillated field. Therefore, we assume that the phase has an independent and uniform distribution, i.e., $f_0(E_0, \phi_0) = (1/2\pi)\rho(E_0)$. In this case, we obtain

$$g_1(\Delta E_1) = \frac{1}{2\pi} \int \rho(E_0) dE_0 \frac{1}{|\partial\Delta E_1/\partial\phi_0|}. \quad (7)$$

According to Eq. (6), v and E_0 satisfy the relativistic relation $v = c\sqrt{1 - m^2c^4/E_0^2}$. However, the analytical recurrence relation for cascaded units becomes highly nonlinear, and it is impractical to derive the optimal parameters. Thus, in the following studies, the Monte Carlo method is employed to optimize the parameters of 100 units.

In a simplified design, the length of each unit is set to be identical while the gap length between adjacent units is changed to control the relative arrival time (i.e., the phase) of electrons entering each unit. Meanwhile, the wave vector of each unit is optimized to achieve the STM condition. We set a threshold of energy gain and the objective of the optimization is the number of electrons that could be accelerated above the threshold. Figure 2(b) shows the proportion of the electrons that could reach the threshold, and we found that the proportion decreases with increasing threshold. This is because the theoretical upbound of energy gain by 100 units is limited to 260 keV according to Eq. (3). The results indicate that as high as 30% of the input electrons could be accelerated to half of the upbound. For typical thresholds of 150 keV and 200 keV, which correspond to atom velocity acceleration from $0.695c$ to $0.805c$ and $0.827c$, where c is the vacuum light velocity, details of the final energy distribution of output electrons

are plotted in Fig. 2(c). The results show that with a device total length less than 6 mm, the electrons could be accelerated to $0.805c$ and $0.827c$ with probabilities of 26.7% and 6.9%, respectively. We also found that although the acceleration is probabilistic for the ensemble, the accelerated electrons have a very narrow energy spectrum and thus are distinguishable from others [as shown by the red and blue shadow in Fig. 2(c)], in sharp contrast to the broad output energy distribution by a single acceleration unit [25,26] or an array of periodically aligned acceleration units [11,12]. The output electrons with energies above the threshold could be almost deterministically selected by choosing an appropriate time window. The multistage acceleration is also investigated with parameters from the Winderoe synchronicity condition [31,42], as shown by the dashed lines in Fig. 2(c), and the output has distributions much broader than those results with numerically optimized parameters. Although more electrons can be accelerated (with probabilities of 19.5% and 18.5% for $0.805c$ and $0.827c$, respectively), the synchronicity condition could not guarantee optimal results since there are a huge number of controllable parameters. Setting the parameters from synchronicity as the initial parameter set and then numerically optimizing them might be a more practical strategy for further improving the performance of the multistage accelerator.

To interpret the cooperation of these units for massive particle acceleration, we plot the detailed average energy and standard deviation of energy (σ_E) and phases (σ_ϕ) at different units in Fig. 3 for the output electrons whose energy gain exceeds 200 keV. The general trend is the same as those parameters obtained from the synchronicity condition. We call them acceleration units, where the average energy of the electron ensemble continuously increases. However, the parameters also show sudden jumps in Fig. 3(c), which deviate from the synchronicity condition, and the average energy in these units usually remains unchanged or decreases. As shown by the orange shadow in Figs. 3(a)–3(c), jumps in the wave vector always correspond to the change in σ_E and have an influence on σ_ϕ . We conjecture that these jumps are aimed at compressing the electron ensemble for narrower energy and phase distributions. Thus, these units are named as “focus units.” In the whole process, acceleration units cause accumulation of energy gain and divergence of the phase of electrons. Thus several focus units are introduced to compress the electrons and make most of them satisfy STM conditions (see Appendix D for more analysis).

Furthermore, the states of the ensemble that enter certain units are depicted by the Poincaré surface of section (SOS) to provide an intuitive interpretation of the electrons’ evolution in two types of units. Figure 4 shows the distributions of the energy and the phase of each electron when entering the 25th, 50th, 75th, and 100th units. The nonlinear mapping of the electron state gives rise to

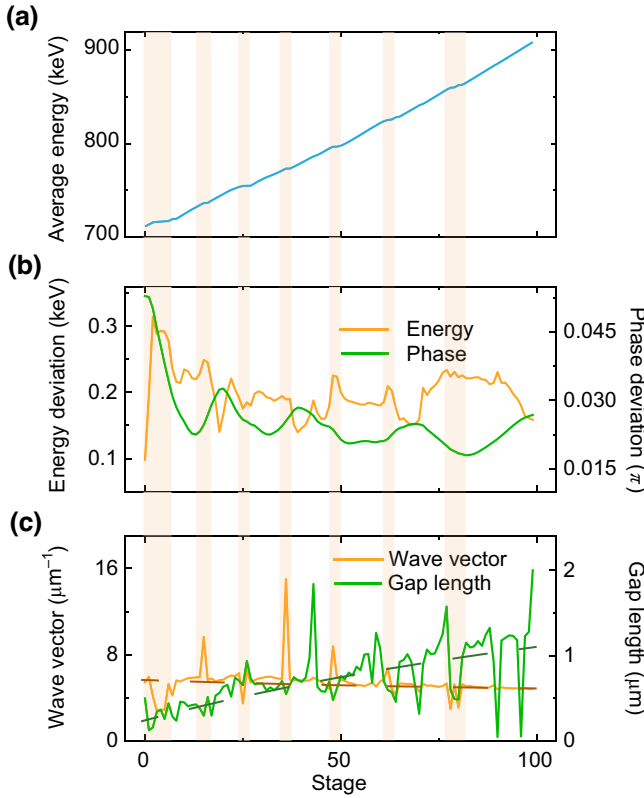


FIG. 3. (a) The evolution of the average energy for electrons in the multistage accelerator, with the parameters of each unit optimized for a target energy gain of 200 keV. (b) The standard deviations of energy and phases for the electrons. (c) Parameters of each unit from the numerical optimization (solid lines) in comparison with those derived from the synchronicity condition (dashed lines).

chaotic manifolds in the phase space, and a bunch of dots at the rightmost (in the red circle) corresponding to the portion of electrons could be effectively accelerated, while the remaining electrons are randomly distributed in the phase. In the SOS, as indicated by the background color in Fig. 4, electrons could be accelerated (in the red region) while decelerated (in the blue region) depending on their phase when entering each unit. In focus units, such as the 25th and 50th units [Figs. 4(a) and 4(b)], the small ensemble of electrons is located at the position off the center of the red or blue area to focus their states into a smaller region, while in acceleration units, such as the 75th and 100th units [Figs. 4(c) and 4(d)], electrons located at the center of the red area could obtain an optimal energy gain. Therefore, a balance between focusing and acceleration eventually gives rise to a narrow energy distribution of output electrons.

IV. CONCLUSION

In conclusion, we generalize the theory of spatial-temporal modulation of optical photons on a photonic chip

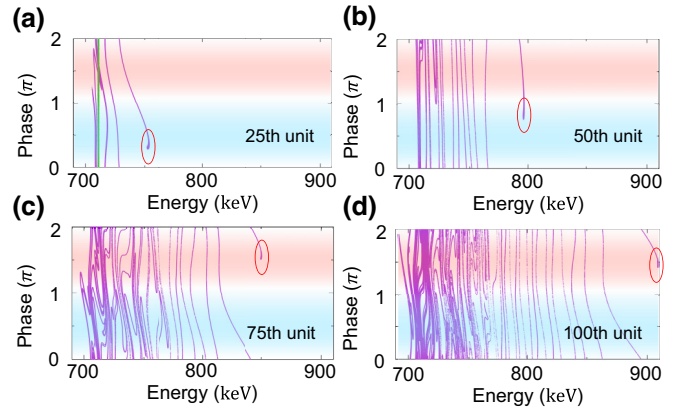


FIG. 4. Phase-space representation of the electron ensemble when entering the 25th (a), 50th (b), 75th (c), and 100th (d) units. The green line in (a) shows the initial distribution of electrons. The parameters of each unit are optimized for a target energy gain of 200 keV, and the other parameters are the same as those in Fig. 2(b). The red and blue areas correspond to the parameter regimes where electrons are accelerated and decelerated, respectively.

to massive particles. With this universal principle, we built a connection between conventional on-chip devices for manipulating photons and very compact and efficient electron accelerators. Through numerically optimizing device parameters, electrons could be accelerated by 150 keV with the probability of 26.7% with a device length less than 6 mm. Spatial-temporal modulation could also be applied to other massive particles. For example, we proposed an integrated atom slower by a series of on-chip optical dipole trap tweezers (Appendix A).

We note that the connection between the on-chip spatial-temporal modulation and massive particle manipulation could also bring alternative ideas to the photonic community, such as the design of an integrated photon frequency modulator overcoming the limitation of dispersion by using the synchronicity condition of conventional electron accelerators (Appendix B).

ACKNOWLEDGMENTS

This work was funded by the National Key Research and Development Program (Grant No. 2021YFF0603701), the National Natural Science Foundation of China (Grants No. 11874342, No. 11922411, No. 12104441, and No. U21A6006), Anhui Provincial Natural Science Foundation (Grant No. 2108085MA22), and the Fundamental Research Funds for the Central Universities. The numerical calculations in this paper were partially done on the supercomputing system in the Supercomputing Center of the University of Science and Technology of China. This work was partially carried out at the USTC Center for Micro and Nanoscale Research and Fabrication.

APPENDIX A: ATOM COOLING

The spatial-temporal modulation for massive particle acceleration can also be adapted for atom cooling by modulating the spatial-temporally dependent optical dipole potential on a photonic chip. For example, a Gaussian beam of a 880-nm laser, with a wavelength 100-nm longer than the D2 transition of the rubidium atoms, could provide an attractive dipole potential for the rubidium atoms. As schematically shown in Fig. 5(a), integrated grating couplers [44] can convert the waveguide mode to a free-space Gaussian beam (waist W) above the chip, with the laser amplitude in the waveguide periodically modulated as $\mathcal{E}(t) = 0$ for $-2\sigma \leq t < 0$ and $\mathcal{E}(t) = \exp[-t^2/\sigma^2]$ for $0 \leq t < 2\sigma$, with a period of 4σ [see Fig. 5(b)]. For the laser frequency largely detuned from the atomic transition, the beams generate trap potential for atoms via the ac-Stack effect that shifts the ground-state energy as

$$U = \frac{2\hbar\Delta\Omega_R^2(t)}{4\Delta^2 + \Gamma^2 + \Omega_R^2(t)}, \quad (\text{A1})$$

where $\Omega_R(t) = d\mathcal{E}(t)/\hbar$ and d is the dipole moment for the atomic transition. Therefore, the Gaussian beam can change the atom's kinetic energy as

$$\delta E(t_0, t_1) = - \int_{t_0}^{t_1} \frac{4\hbar\Omega_R^2(t)\Delta v |x_0 + vt|}{[4\Delta^2 + \Gamma^2 + \Omega_R^2(t)] W^2} dt, \quad (\text{A2})$$

where v is the velocity of the atom and x_0 corresponds to the atom position at t_0 with respect to the center of the Gaussian beam.

Considering precooled ^{87}Rb atom ensembles, with an initial average velocity of 10 m/s and a standard deviation of 0.0625 m/s, we could use the chip [as depicted in Fig. 5(a)] for on-chip atom cooling and trapping. By the spatial-temporal modulation scheme shown in Fig. 5(b), the STM could be realized by optimizing the switching time T , which could be controlled by the on-chip delay and σ , with the two parameters corresponding to the phase and wave vector in Fig. 2 of the main text. The other parameters are fixed, with the laser waist, maximum potential depth, and distance between two adjacent gratings being 1.5 μm , 3.5 mK, and 7.5 μm , respectively. Similar to the electron accelerator, we assume a device composed of 200 units, with T and σ that can be optimized for each stage. The results of atom trapping are summarized in Fig. 5(c). By such an approximately 2-mm-long photonic device on a chip, atoms can be cooled down and trapped with a probability of approximately 27% in the last ten stages.

APPENDIX B: PHOTON FREQUENCY SHIFT

Under spatial-temporal modulation, the refractive index of a waveguide is inhomogeneous, and the head of a wavepacket (pulse) may travel slower (faster) than its tail,

which will induce a frequency shift [41]. Choosing two points in the wavepacket separated by a wavelength, the shift of the local wavelength is

$$d\lambda = \Delta v dt = - \frac{c}{n_{\text{eff}}^2} \frac{\partial \Delta n_{\text{eff}}(x, t)}{\partial x} \lambda \frac{n_{\text{eff}}}{c} dx \quad (\text{B1})$$

where n_{eff} is the effective refractive index of the waveguide, $\Delta n_{\text{eff}}(x, t)$ is the mechanically induced spatial-temporal modulation of n_{eff} , c is the speed of light in vacuum, and λ is the wavelength of photons, which is assumed to be a constant in a single unit. Specifically,

$$d\lambda = -v_g \frac{2\pi}{\omega} \frac{\partial \Delta n_{\text{eff}}(x, t)}{\partial x} dx, \quad (\text{B2})$$

where v_g is the light group velocity in the waveguide and ω is the angular frequency of light. Then, the frequency shift can be derived as

$$d\omega = v_g \frac{2\pi}{\lambda} \frac{\partial \Delta n_{\text{eff}}(x, t)}{\partial x} dx = v_g k_0 \frac{\partial \Delta n_{\text{eff}}(x, t)}{\partial x} dx, \quad (\text{B3})$$

where $k_0 = 2\pi/\lambda$ is the optical wave vector in vacuum. As the frequency shift is an adiabatic process, which means that the amplitude change of the electromagnetic wave is very slow compared to the frequency of photons, the photon number is conserved [45]. Thus, $dE = \hbar d\omega$, with \hbar being the reduced Planck constant. We obtain the total energy change in a single unit as

$$\delta E \approx \hbar v_g k_0 \int d\zeta \frac{\partial}{\partial x} [\Delta n_{\text{eff}}(x, t)]. \quad (\text{B4})$$

Here, the integration is along the trajectory ζ from the initial wavepacket position $\{x_0, t_0\}$ to the final wavepacket position $\{x_1, t_1\}$, as in the main text.

The Wideroe synchronicity condition [42] is also helpful for further study in optical frequency modulators, as the dispersion characteristics of light are considerable when the frequency shift is increasingly strong. In a section of the suspended optical waveguide, a time-dependent mechanical deformation can change the optical length and lead to compression or stretching of photons, which results in a frequency shift. For a periodic mechanical deformation, the frequency shift of a photon determined by its input phase ϕ and the interaction length L is [41]

$$\delta\omega = -A \left[\sin\left(\phi - \frac{\omega L}{2v_g}\right) - \sin\left(\phi + \frac{\omega L}{2v_g}\right) \right], \quad (\text{B5})$$

where A , ω_m , v_p are the frequency shift coefficient, the angular frequency of the mechanical deformation, and the group velocity of the waveguide, respectively. Such a process is reminiscent of a particle in a standing-wave accelerator. Thus, "drift tubes" [42] could be introduced to

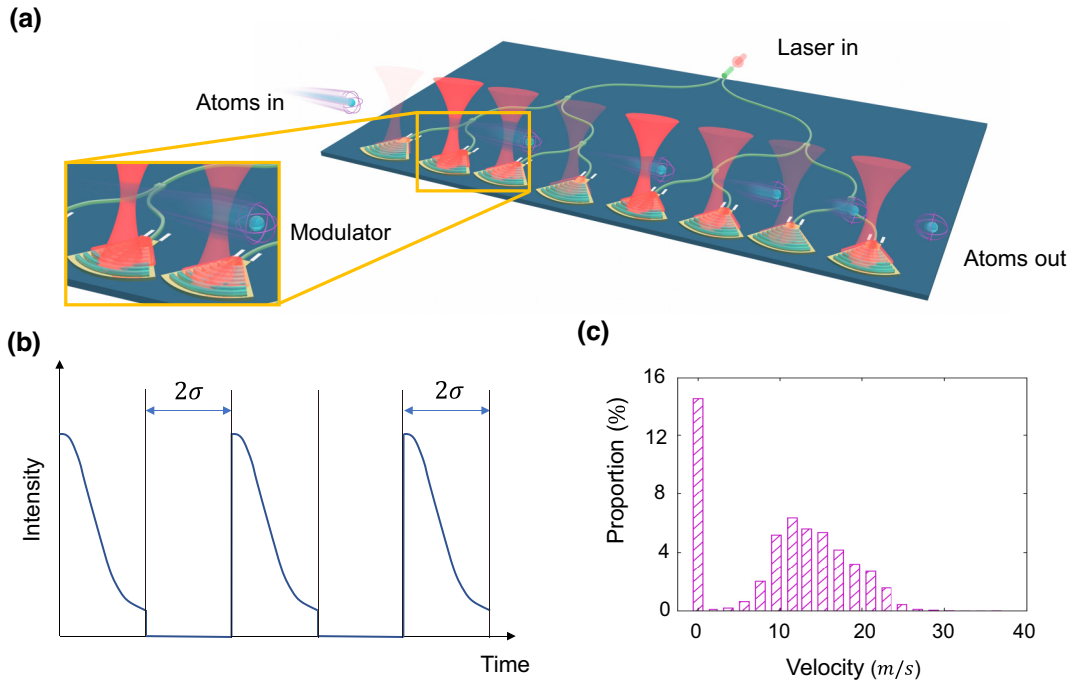


FIG. 5. (a) Sketch of the experimental setup for cascaded atom decelerator on a photonic chip. Atoms are emitted from the left, and they interact with the spatial-temporally modulating dipole trap potential, which is generated by Gaussian beams from the on-chip grating couplers. (b) The time-dependent intensity of input lasers to the gratings. The laser is modulated to be a series of pulses of half Gaussian function shape, with the standard deviation of the Gaussian function being σ . (c) Histogram statistic for the velocity of an ensemble of atoms after deceleration. The central electric field is 2×10^6 V/m, the gap length is set at $7.5 \mu\text{m}$, the laser detuning with respect to the atomic transition is 100 nm. The total number of atoms in the ensemble is 10 000 with initial velocities following a Gaussian distribution, which is centered at 10 m/s with a standard deviation of 0.0625 m/s.

maintain the synchronicity condition between the optical photons and mechanical deformation. For photons whose dispersion can be ignored, their group velocity can be treated as a constant, thus the “drift tubes” have a fixed length $G = \pi v_g / \omega_m$. To obtain the maximum energy in a certain length, the interaction length L is always set as the same as the length of the “drift tube,” which corresponds to the so-called quasi-phase-matching condition in nonlinear optics [46]. However, when the dispersion of the waveguide is large enough, which means that the phase difference between photons with different frequencies is comparable to π in the acceleration process, identical “drift-tube” lengths are inappropriate. As shown in Fig. 6(a), the achievable maximum frequency shift is limited and cannot be further increased by adding more stages. When the Wideroe synchronicity condition is introduced and satisfied in this system, this limitation can be overcome, as illustrated in Fig. 6(b). In addition, the performances of the optical frequency shifter based on the Wideroe synchronicity condition are tested with typical devices, including waveguides (large dispersion) and optical fibers (small dispersion), and the results are shown in Fig. 6(c). With the synchronicity condition, the final distribution of the photons becomes asymmetric, and the maximum frequency shift will constantly increase by adding more units. It

should also be noted that the distribution around the maximum frequency is broad, which can be compressed by further optimizing the parameters.

APPENDIX C: CORRESPONDENCES BETWEEN THE ACCELERATOR PHYSICS AND WAVE OPTICS

In this section, we build the correspondence between the massive particle accelerator and the optical frequency modulator. From the perspective of wave dynamics, the process in which a single electron propagates in the accelerator can be treated as the manipulation of matter waves in analogs to the modulation of electromagnetic waves in the optical waveguide. In the following, we will show the correspondences by analyzing the evolution of the electron wave function and the light field distribution. For example, the Wideroe synchronicity condition for the electron acceleration process corresponds to the phase matching (quasi-phase-matching) condition for the optical field modulation process. In Table I, more details about the correspondences are summarized.

In the following, we provide detailed derivations about the correspondences.

TABLE I. Correspondences between the electrons acceleration and optical field modulation.

Accelerator physics	Wave optics
Wave function	Amplitude distribution
$\psi(z, t) = \phi(z, t) e^{i \frac{p_0}{\hbar} z - i \frac{E_0}{\hbar} t}$	$A(z, t) = a(z, t) e^{i k_0 z - i \omega_0 t}$
Energy-momentum relation	Dispersion relation
$E = E_0 + v_0(p - p_0) + \frac{1}{2m}(p - p_0)^2$	$\omega = \omega_0 + v_g(k - k_0) + \frac{1}{2} \left(\frac{\partial^2 \omega}{\partial k^2} \right)_{k_0} (k - k_0)^2$
Evolution without interaction	Evolution without interaction
$\psi(z, t) = \phi'_0 e^{i \left(\frac{p_0}{\hbar} z - \frac{E_0}{\hbar} t \right)} e^{-\frac{(z - v_0 t)^2}{2(\sigma_z^2 + i \frac{\hbar t}{m})}}$	$A(z, t) = a'_0 e^{i(k_0 z - \omega_0 t)} e^{-\frac{(z - v_g t)^2}{2(\sigma_z^2 + i \left(\frac{\partial^2 \omega}{\partial k^2} \right)_{k_0} t)}}$
Schrodinger equation with interaction	Propagation equation with interaction
$2 \frac{\partial \phi(z, t)}{\partial z} + \frac{1}{v_g} \frac{\partial \phi(z, t)}{\partial t} = \frac{i}{\hbar} \int_0^t \frac{\partial U(z, t')}{\partial z} dt' \phi(z, t)$	$2 \frac{\partial a(z, t)}{\partial z} + \frac{1}{v} \frac{\partial a(z, t)}{\partial t} = i \int_0^t \frac{\partial U_{\text{eff}}(z, t')}{\partial z} dt' a(z, t)$
Energy change due to the interaction	Frequency shift due to the interaction
$\delta E = - \int \frac{\partial U(z, t)}{\partial z} d\zeta$	$\delta \omega = - \int \frac{\partial U_{\text{eff}}(z, t)}{\partial z} d\zeta$
Wavepacket deformation due to the interaction	Wavepacket deformation due to the interaction
$\sigma_E = - \int \frac{\partial^2 U(z, t)}{\partial z \partial t} d\zeta$	$\sigma = - \int \frac{\partial^2 U_{\text{eff}}(z, t)}{\partial z \partial t} d\zeta$
Evolution with interaction	Evolution with interaction
$\psi \left(z, \frac{L}{v_0} \right) = \phi(z - L, 0) e^{i \frac{1}{\hbar} [p_0 z - (E_0 + \delta E) t - \frac{1}{2} \sigma_E t^2]}$	$A \left(z, \frac{L}{v_g} \right) = a(z - L, 0) e^{i [k_0 z - (\omega_0 + \delta \omega) t - \frac{1}{2} \sigma t^2]}$
Synchronicity condition for traveling-wave accelerator	Phase-matching condition
$v = \frac{\omega_r}{k_r}$	$k_0 = \sum_i k_i$
Synchronicity condition for standing-wave accelerator	Quasi-phase-matching condition
$\frac{\omega_r}{v_n} (L + G_n) = 2h\pi, h \in N$	$\frac{\Omega}{v_{gn}} (L + G_n) = 2h\pi, h \in N$

1. The wave-function description

The wave function for an electron propagating along the z direction with a center energy E_0 and a momentum p_0 can be expressed as

$$\psi(z, t) = \phi(z, t) e^{i \frac{p_0}{\hbar} z - i \frac{E_0}{\hbar} t}. \quad (\text{C1})$$

Similarly, the optical field propagating along the z direction with a center angular frequency ω_0 and a wave vector k_0 can be written as

$$A(z, t) = a(z, t) e^{i k_0 z - i \omega_0 t}. \quad (\text{C2})$$

Here we ignore the relativistic effect, and expand the self-energy according to the momentum around the center energy:

$$E = E_0 + v_0(p - p_0) + \frac{1}{2m}(p - p_0)^2, \quad (\text{C3})$$

where E, p are the self-energy and momentum, respectively, $v_0 = p_0/m$ is the center velocity and m is the mass

of the electron. For the optical field in an optical waveguide, there is a similar relation between the frequency and wave vector

$$\omega = \omega_0 + \left(\frac{\partial \omega}{\partial k} \right)_{k_0} (k - k_0) + \frac{1}{2} \left(\frac{\partial^2 \omega}{\partial k^2} \right)_{k_0} (k - k_0)^2 + O((k - k_0)^3), \quad (\text{C4})$$

where ω, k are the angular frequency and wave vector. The term $(\partial \omega / \partial k)_{k_0} = v_g$ is the group velocity and $(\partial^2 \omega / \partial k^2)_{k_0} = 1/\beta$ is caused by the group-velocity dispersion (GVD).

2. The propagation of wave packet

The evolution of the wave function of the electron and the amplitude distribution of the optical field can be decomposed into two types: (i) evolution without modulation from the external field, and (ii) evolution under external potential field modulation.

We first consider the evolution without modulation from an external field. When the initial wave function of the

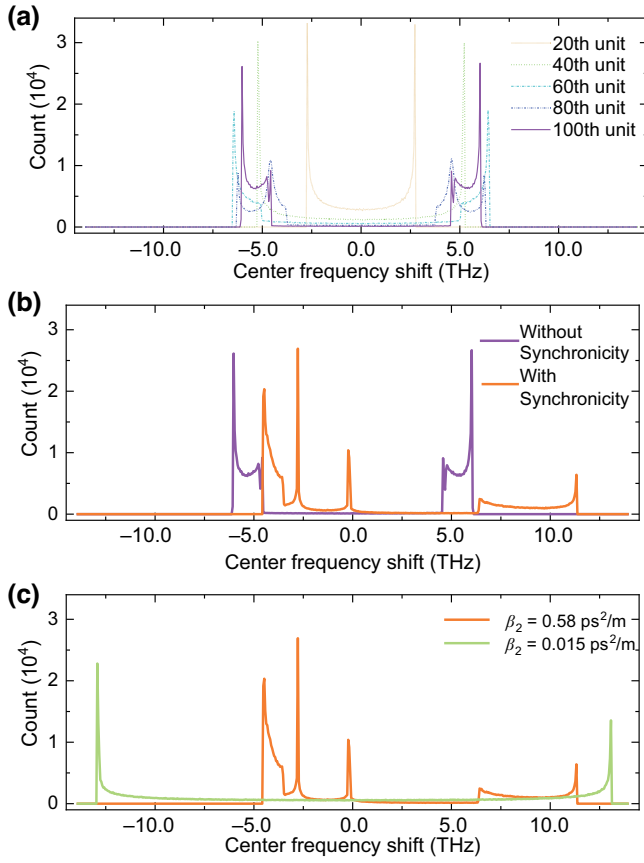


FIG. 6. The final frequency distribution of output photons for 500 000 input photons, with an input central frequency of 194 THz and the initial phases are randomly distributed. (a) With the frequency shift coefficient $A = 106.8$ GHz, length of the unit $L = 9.1$ mm, group-velocity deviation $\beta_2 = 0.58$ ps²/m and initial group velocity $v_g = c/2$, where c is the speed of light in vacuum. The frequency is symmetrically shifted as the number of units increases. (b) The results for the parameters optimized with and without the Wideroe synchronicity condition, with a synchronicity phase $\phi_s = \arcsin 0.7$. (c) The results considering the dispersion for a typical waveguide (orange line, $\beta_2 = 0.58$ ps²/m) and optical fiber (green line, $\beta_2 = 0.015$ ps²/m), with the parameters from the Wideroe synchronicity condition. In these plots, 194 THz is taken as the reference point for the center frequency shift, and the frequency interval is 0.5 keV.

electron is a Gaussian function $\phi(z, 0) = \phi_0 e^{z^2/2\sigma_z^2}$, the evolution of the wave function in free space according to the Schrodinger equation reads

$$\psi(z, t) = \phi'_0 e^{i\left(\frac{p_0}{\hbar}z - \frac{E_0}{\hbar}t\right)} e^{-\frac{(z-v_0t)^2}{2(\sigma_z^2 + i\frac{\hbar t}{m})}}, \quad (\text{C5})$$

where ϕ'_0 is a normalization factor. The center of the wavepacket is v_0t , which means that the electron propagates along the z direction with a velocity of v_0 . Since the components of the wave function with different self-energy correspond to different velocities, we expect that the shape

of the packet will deform while propagating along the z direction. As shown in the wave function, the standard deviation of the packet becomes $\sqrt{\sigma_z^2 + i(\hbar t/m)}$, which means that the packet is broadened and the broaden speed is depends on $1/m$.

In comparison, for an initial optical field of a Gaussian pulse $a(z, 0) = a_0 e^{-(z^2/2\sigma_z^2)}$, when there is no external field modulating the pulse, the evolution of the optical field can be written as

$$A(z, t) = a'_0 e^{i(k_0z - \omega_0t)} e^{-\frac{(z-v_g t)^2}{2(\sigma_z^2 + i\frac{\hbar t}{\beta})}}, \quad (\text{C6})$$

where a'_0 is the normalization constant. The pulse propagates along the z direction with the group velocity $v_g = (\partial\omega/\partial k)_{k_0}$, similar to the electron, since the center position of the packet is $v_g t$. Unlike light in free space, there is a GVD in the waveguide for the optical field, which means that the group velocity of the field is dependent on its frequency. Thus, the shape of the wavepacket will change similar to the wave function of the electron. Its standard deviation becomes $\sqrt{\sigma_z^2 + i(t/\beta)}$, meaning that the broadening of the packet is related to the term $[(1/\beta)(\partial^2\omega/\partial k^2)]_{k_0}$, which is nonzero for optical fields in waveguide.

Now, we discuss the case with spatial-temporal modulation. For the electron, the evolution of the wave function in a spatially and temporally varying potential field $U(z, t)$ can be solved by treating the spatial-temporal modulation process as a perturbation, i.e., the self-energy change in the process δE is far smaller than the self-energy of the particle, the Schrodinger equation can be linearized as [33]

$$\frac{\partial\phi(z, t)}{\partial z} + \frac{1}{v_g} \frac{\partial\phi(z, t)}{\partial t} = \frac{i}{\hbar} \int_0^t \frac{\partial U(z, t')}{\partial z} dt' \phi(z, t), \quad (\text{C7})$$

where $U(z, t)$ is the potential field. The evolution of the wave function is

$$\begin{aligned} \phi(z, t) &= \phi(z - v_0t, 0) e^{i\frac{1}{\hbar} \int_0^t \int_0^t \frac{\partial U(z, t')}{\partial z} dt' dz} \\ &= \phi(z - v_0t, 0) e^{i\frac{1}{\hbar} \int_0^t \int_0^t \frac{\partial U(z, t')}{\partial z} dz dt'}, \end{aligned} \quad (\text{C8})$$

where the integration $\int_{(z-v_0t, 0)}^{(z+v_0(t-t), t)}$ $(\partial U(z, t)/\partial z) dz$ is along the trajectory ζ .

For optical fields under modulation, the optical propagation function can be written as [17,41]

$$\frac{\partial a(z, t)}{\partial z} + \frac{1}{v_g} \frac{\partial a(z, t)}{\partial t} = \frac{i}{\hbar} \int_0^t \frac{\partial U_{\text{eff}}(z, t')}{\partial z} a(z, t), \quad (\text{C9})$$

where $U_{\text{eff}}(z, t)$ is the effective potential field and $-i/\hbar \int_0^t \partial U_{\text{eff}}(z, t')/\partial z = \delta\beta(z, t)$ is the change in the wave vector. The evolution of the amplitude distribution is

$$a(z, t) = a(z - v_g t, 0) e^{i\frac{1}{\hbar} \int_0^t \int_0^t \frac{\partial U_{\text{eff}}(z, t')}{\partial z} dz dt'}. \quad (\text{C10})$$

3. The matching condition

Furthermore, since the wavepacket of a single electron is much smaller than the scale of the interacting area, the electron accelerator system always corresponds to the short pulse in the optical system. Because the length of the accelerator unit is L , the wave function is

$$\psi\left(z, \frac{L}{v_0}\right) \approx \phi(z-L, 0)e^{i\frac{1}{\hbar}\left[p_0z - (E_0 + \delta E)t - \frac{1}{2}\sigma_E t^2\right]}, \quad (\text{C11})$$

where $\delta E = -\int_{(z-L, 0)}^{(z, L/v_0)} (\partial U(z, t)/\partial z) d\zeta$; $\sigma_E = -\int_{(z-L, 0)}^{(z, L/v_0)} (\partial^2 U(z, t)/\partial z \partial t) d\zeta$. To gain maximum energy in the process, the term $-\int_{(z-L, 0)}^{(z, L/v_0)} (\partial U(z, t)/\partial z) d\zeta$ should take the maximum value, which is our spatial-temporal matching (STM) condition. Here, the STM condition can also be generalized to take the maximum value of $-\int_{(z-L, 0)}^{(z, L/v_0)} (\partial^2 U(z, t)/\partial z \partial t) d\zeta$ along the trajectory, which can be used to modulate the shape of the particle wave function. For a pulse whose duration time t_d is much shorter than the interacting time L/v_g , the field can be approximately expressed as

$$A\left(z, \frac{L}{v_g}\right) \approx a(z-L, 0)e^{i\left[k_0z - (\omega_0 + \delta\omega)t - \frac{1}{2}\sigma t^2\right]}, \quad (\text{C12})$$

where $\delta\omega = -1/\hbar \int_{(z-L, 0)}^{(z, L/v_g)} (\partial U_{\text{eff}}(z, t)/\partial z) d\zeta$ and $\sigma = -1/\hbar \int_{(z-L, 0)}^{(z, L/v_g)} (\partial^2 U_{\text{eff}}(z, t)/\partial z \partial t) d\zeta$. In an optical system, keeping $\delta\omega$ at its maximum will lead to the satisfaction of the STM condition and give the maximum frequency shift.

When the exact form of the potential fields $U(z, t)$ and $U_{\text{eff}}(z, t)$ is provided, the STM condition $-\int_{(z-L, 0)}^{(z, L/v_0)} (\partial U(z, t)/\partial z) d\zeta$ and $-\int_{(z-L, 0)}^{(z, L/v_g)} (\partial U_{\text{eff}}(z, t)/\partial z) d\zeta$ take the maximum value will lead to the corresponding synchronicity condition and phase-matching condition. When $U(z, t)$ and $U_{\text{eff}}(z, t)$ are corresponding to a traveling-wave field, STM conditions lead to the synchronicity condition for the moving wave accelerator and phase-matching condition. For an electron interacting with a moving wave electric field, the potential can be written as

$$U(z, t) = -E_0 \frac{1}{k_r} \cos(k_r z - \omega_r t + \phi), \quad (\text{C13})$$

where E_0 , k_r , and ω_r are the strength, wave vector, and angular frequency of the electric field, respectively. For an interaction length L , we have

$$\begin{aligned} & -\int_{(z-L, 0)}^{(z, L/v_0)} \frac{\partial U(z, t)}{\partial z} d\zeta = E_0 \\ & \times \text{sinc}\left[\left(\frac{\omega_r}{v_0} - k_r\right)L/2\right] L \sin(\phi_0). \end{aligned} \quad (\text{C14})$$

When $v_0 = \omega_r/k_r$ and $\phi_0 = k_r(z-L) + \phi = (\pi/2) + 2\pi h$, $h \in \mathbb{N}$, the STM condition is satisfied. Condition

$v_0 = \omega_r/k_r$ means that the velocity of the electron is equal to the phase velocity of the external electric field and the relative position of the electron to the potential field is fixed. When the proper initial relative position ϕ_0 is chosen, the electron constantly feels the maximum acceleration force in the process. Under STM condition, the energy change is $\delta E = E_0 L$, which is proportional to the interaction length L . In the optical field modulator, several moving waves with different angular frequencies ω_i and wave vectors k_i cause perturbation of the reflex index of the waveguide. Thus, the change in the wave vector has the form of $\delta k(z, t) = A \cos(\sum_i k_i z - \sum_i \omega_i t + \phi)$, where A is the modulation strength [39]. The effective potential is

$$U_{\text{eff}}(z, t) = -A \frac{\sum_i \omega_i}{\sum_i k_i} \cos\left(\sum_i k_i z - \sum_i \omega_i t + \phi\right). \quad (\text{C15})$$

For an interaction length L , we have

$$\begin{aligned} & -\int_{(z-L, 0)}^{(z, L/v_0)} \frac{\partial U_{\text{eff}}(z, t)}{\partial z} d\zeta = AL \sin(\phi_0) \sum_i \omega_i \\ & \times \text{sinc}\left[\left(\frac{\sum_i \omega_i}{v_g} - \sum_i k_i\right)L/2\right]. \end{aligned} \quad (\text{C16})$$

When $(\sum_i \omega_i/v_g) - \sum_i k_i = 0$ and $\phi_0 = \sum_i k_i(z-L) + \phi = (\pi/2) + 2\pi h$, the STM condition is satisfied. With the linear dispersion relation, the phase velocity is equal to the group velocity, thus $v_g = v_{\text{phase}} = \omega_0/k_0$. With energy conversion, $\omega_0 = \sum_i \omega_i$. Thus, we have the relation $k_0 = \sum_i k_i$, which is the phase-matching condition. Under STM condition, the frequency shift $\delta\omega = A\omega_0 L$, similar to the energy change for electrons, is also proportional to the interaction length L .

When $U(z, t)$ and $U_{\text{eff}}(z, t)$ are corresponding to a standing-wave field, STM conditions lead to the synchronicity condition for the standing-wave accelerator, i.e., Wideroe synchronicity condition, and quasi-phase-matching condition. For a standing-wave accelerator, the potential can be written as $U(z, t) = -E_0 z \cos(\omega_r t + \phi)$, and

$$-\int_{(z-L, 0)}^{(z, L/v_0)} \frac{\partial U(z, t)}{\partial z} d\zeta = E_0/\omega_r \sin\left(\frac{\omega_r}{v_0} L/2\right) \sin(\phi_0), \quad (\text{C17})$$

which oscillates with increasing interaction length. By adding some gaps with a length of G_n to separate the

interaction area into N units with a length of L , we have

$$\begin{aligned}
 & - \int_{(z_0,0)}^{(z_0+\sum_{n=1}^N \frac{L+G_n}{v_n}, \sum_{n=1}^N \frac{L+G_n}{v_n})} \frac{\partial U(z,t)}{\partial z} d\zeta \\
 & = E_0/\omega_r \sin(\phi_0) \sum_{n=0}^{n=N} v_n \sin \left[\left(\frac{\omega_r}{v_n} \right) L/2 \right] \\
 & \times \sin \left(\sum_{n'=0}^{n'=n} \frac{\omega_r}{v_{n'}} (L + G_{n'}) \right), \quad (C18)
 \end{aligned}$$

where v_n is the velocity of the electron in the n th unit. When $\phi_0 = (\pi/2) + 2\pi h$ and $(\omega_r/v_n)(L + G_n) = 2h\pi$ for all n , the STM condition can be satisfied, and the energy change is $E_0 L \sum_{n=0}^{n=N} \text{sinc}[(\omega_r/v_n)L/2]$. It should be noted that $(\omega_r/v)N(L + G) = 2h\pi$ is the Wideroe synchronicity condition for the electron accelerator. For an optical field modulator driven by standing waves, the effective potential field has the form $U_{\text{eff}}(z, t) = -A\Omega z \cos(\Omega t + \phi)$, where Ω is the modulation frequency. There is

$$- \int_{(z-L,0)}^{(z, \frac{L}{v_0})} \frac{\partial U_{\text{eff}}(z, t)}{\partial z} d\zeta = A \sin \left[\frac{\Omega}{v_g} L/2 \right] \sin(\phi_0). \quad (C19)$$

The frequency shift oscillates when the interaction strength increases. Similarly, by adding some gaps with a length of G_n to separate the interaction area into n units with a length of L , we have

$$\begin{aligned}
 & - \int_{(z_0,0)}^{(z_0+\sum_{n=1}^N \frac{L+G_n}{v_n}, \sum_{n=1}^N \frac{L+G_n}{v_n})} \frac{\partial U_{\text{eff}}(z, t)}{\partial z} d\zeta \\
 & = A \sin(\phi_0) \sum_{n=0}^{n=N} v_{gn} \sin \left[\frac{\Omega}{v_{gn}} L/2 \right] \\
 & \times \sin \left(\sum_{n'=0}^{n'=n} \frac{\Omega}{v_{gn'}} (L + G_{n'}) \right), \quad (C20)
 \end{aligned}$$

where v_{gn} is the group velocity of the optical pulse in the n th unit, which varies according to the center frequency of the pulse. When $\phi_0 = (\pi/2) + 2\pi h$ and $(\Omega/v_{gn})(L + G_n) = 2h\pi$ for all n , the STM condition can be satisfied, and the frequency shift $\delta\omega = A\Omega L \sum_{n=0}^{n=N} \text{sinc}[(\Omega/v_n)L/2]$. In most modulation systems, the frequency shift is much smaller than the center frequency of the optical field, thus the linear dispersion approximation can be adopted, where v_g is considered as a constant. In such systems, the length of gap G_n is identical for all the units, and the relation becomes $(\Omega/v_g)(L + G) = 2h\pi$, which is the common form of the quasi-phase-matching condition. Based on the correspondences between accelerator physics and wave optics above, the

well-developed field of optical field modulation will provide some insights to control the electron wave function and investigate the quantum nature of massive particles.

APPENDIX D: CORRESPONDENCES BETWEEN THE ACCELERATOR PHYSICS AND RAY OPTICS

In most multistage acceleration systems, which include a large number of incoherent electrons, the quantum nature of the electrons is hidden. Thus, we also investigated the behavior of the accelerator by treating the electrons as classical point particles traveling in an electric field and using the possibility density function $f(v, \varphi)$, where v, φ is the velocity and relative phase to the potential field of the electrons, to describe the distribution of the electrons. Similar to the correspondences between the electron acceleration process described by the Schrodinger equation and wave optics, there are also correspondences between the classical electron acceleration process and ray optics. The propagation of electrons in a multistage accelerator is similar to the evolution of the rays in an optical system, where the deflection, scattering, and focusing of the ray occur.

As shown in Figs. 7(a) and 7(c), the evolution of the electron ensemble can be divided into two types: (i) evolution in free space and (ii) evolution in the external potential (electric) field. In the ray optics correspondence, the two types correspond to the propagation of light beams in free space and the passing of rays through different optical devices. In the first type of evolution, velocities of the electrons and wave vectors of the rays are kept, and the relative phases of electrons and positions of the rays change according to them. In the second type of evolution, the velocities of the electrons and wave vectors of the rays are modulated according to their relative phases or positions. Thus, the distribution of the electron ensemble in phase-velocity space can be focused and shifted by introducing different types of interaction units, such as the prism and lens in a geometrical optics system. By appropriately arranging different types of interaction units in the multistage accelerator, electrons can be efficiently accelerated while being highly focused in phase-velocity space, as shown in Figs. 7(b1)–7(b7).

Consider the first type of evolution, i.e., the evolution in free space. For the electron to propagate in free for the length of G , there is

$$\begin{aligned}
 v & = v_0 \\
 \varphi & = \varphi_0 + \frac{\omega_r}{v_0} G, \quad (D1)
 \end{aligned}$$

where ω_r is the reference frequency. This means that faster electrons will accumulate less relative phase in the same propagation length, and the initial difference in velocity will cause variation in the distribution of the relative phase, as shown in Figs. 7(b1), 7(b3), 7(b5),

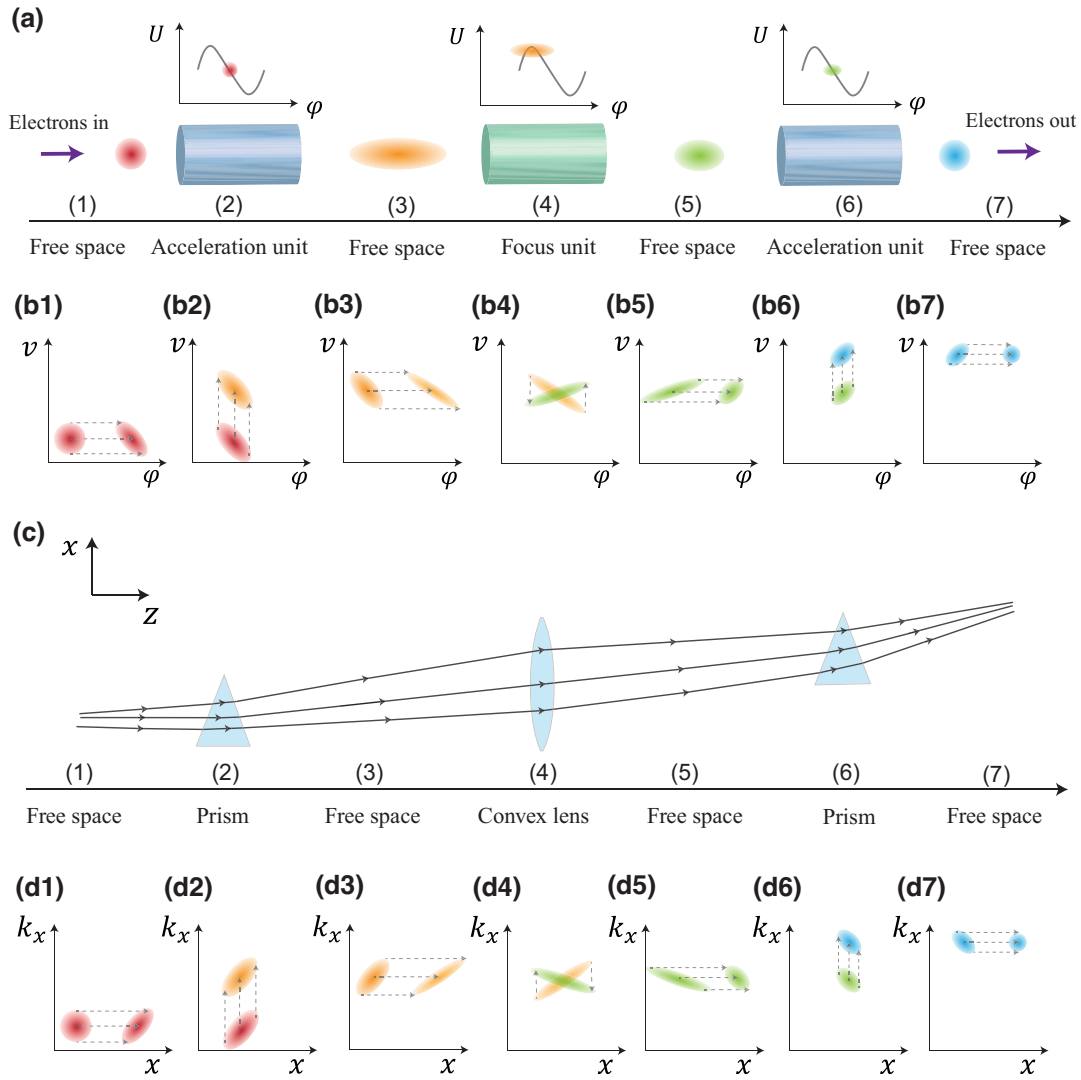


FIG. 7. (a) Schematic diagram for a multistage acceleration process. The process is composed of seven parts from left to right, where the electron ensemble propagates in the free space and passes through the acceleration unit (green cylinder) or focus unit (blue cylinder). Insets show the relative position of the ensemble to the potential field in the acceleration or focus unit, where U is the potential field and φ is the relative phase between electrons and the potential field. (b1)–(b7) The evolution of the possibility density function of the electron ensemble in the corresponding part of the acceleration process in (a), where the darkness represents possibility density and the change of color marks the part where the ensemble passes through the acceleration unit or focus unit. (c) Schematic diagram for a geometrical optics process from left to right, where the optical axis is along the z direction and the rays are deflected along the x direction. The process is composed of seven parts, where a beam of light rays propagates in the free space and passes through the prism or convex lens. (d1)–(d7) The evolution of the intensity distribution function of the rays in the corresponding part of the geometrical optics process in (c), where the darkness represents intensity and the change of color marks the part where the rays pass through the prism or lens. Here, x is the position of the front of the ray, and k_x is the x component of the wave vector of the ray.

and 7(b7). For the initial Gaussian distribution $f_0(v, \varphi) = N_0 e^{-\frac{(\varphi - \varphi_0)^2}{\sigma_\varphi^2} - \frac{(v - v_0)^2}{\sigma_v^2}}$, N_0 is the normalization constant, and σ_φ and σ_v are the deviations of the phase and velocity, respectively. After propagating for the length of G , the probability density function becomes

$$f_1(v, \varphi) = N_1 \exp \left[-\frac{\left(\varphi - \varphi_0 - \frac{\omega_r}{v} G\right)^2}{\sigma_\varphi^2} - \frac{(v - v_0)^2}{\sigma_v^2} \right], \quad (\text{D2})$$

where N_1 is a normalization factor. By defining $\delta\varphi = \varphi - \varphi_1$ and $\delta v = v - v_1$, where $\varphi_1 = \varphi_0 + (\omega_r/v_0)G$ and $v_1 = v_0$, the probability density function can be written as

$$f_1(\delta v, \delta\varphi) = N_1 \exp \left[-\frac{\left(\delta\varphi + \frac{\omega_r}{v_0^2} G \delta v\right)^2}{\sigma_\varphi^2} - \frac{\delta v^2}{\sigma_v^2} \right], \quad (\text{D3})$$

which means the standard deviation of the phase is increased while the deviation of the velocity stays unchanged for a bunch of electrons. The center point of the phase and velocity becomes $\varphi_1 = \varphi_0 + (\omega_r/v_0)G$, $v_1 = v_0$. The standard deviation of the relative phase is increased to $\sigma_\varphi \sqrt{1 + (\sigma_v^2 \omega_r^2 G^2 / \sigma_\varphi^2 v_0^4)}$, which is related to the deviation of velocity σ_v and propagation length G .

As shown in Fig. 7(c), in the geometrical optics system, where the optical axis is along the z direction, a light beam has a similar evolution process. For a light beam starting from the point (z_0, x_0) , where x is the direction vertical to the optical axis and has the wave vector $\vec{k}_0 = (k_{0z}, k_{0x})$, after propagating in the free space for the length of G , its position and wave vector can be written as

$$k_x = k_{0x}, \quad (\text{D4})$$

$$x = x_0 + \frac{k_{0x}}{k_{0z}} G, \quad (\text{D5})$$

where we assume that $G \gg x$, $k_{0z} \gg k_x$. Rays with larger k_{0x} will propagate more distance in the x direction, which is shown in Figs. 7(d1), 7(d3), 7(d5), and 7(d7). In the same way, after propagating in free space for a length of G , the intensity distribution function of the light beam, whose initial distribution is also the Gaussian function $g_0(k_x, x) = N_0 e^{-((k_x - k_{0x})^2 / \sigma_{k_x}^2) - ((x - x_0)^2 / \sigma_x^2)}$, becomes

$$g_1(\delta k_x, \delta x) = N_1 \exp \left[-\frac{\left(\delta x - \frac{G}{k_{0z}} \delta k_x \right)^2}{\sigma_x^2} - \frac{\delta k_x^2}{\sigma_{k_x}^2} \right], \quad (\text{D6})$$

where $\delta k = k_x - k_{1x}$, $\delta x = x - x_1$ and the center point of the phase and velocity becomes $x_1 = x_0 + (G/k_{0z})k_{0x}$, $k_{1x} = k_{0x}$.

Then, we consider the second type of evolution, i.e., evolution in the electric field. With the potential $U(z, t) = -E_0(1/k_n) \cos(k_n z - \omega_r t + \phi_0)$ and interaction length L , there is

$$v = v_0 + \frac{E_0 L}{m v_0} \text{sinc} \left[\left(\frac{\omega_r}{v_0} - k_0 \right) L/2 \right] \sin(\phi_0 + \varphi_0), \quad (\text{D7})$$

$$\varphi = \varphi_0. \quad (\text{D8})$$

For the initial distribution $f_1(v, \varphi) = N_1 \exp \{ -[\varphi - \varphi_0 - (\omega_r/v)G]^2 / \sigma_\varphi^2 - ((v - v_0)^2 / \sigma_v^2) \}$, when the synchronicity condition is satisfied, i.e., $\varphi_0 - (\omega_r/v)G + \phi_0 = (\pi/2) + 2h\pi$ and $(\omega_r/v_0) - k_0 = 0$, the possibility density function

becomes

$$f_2(\delta v, \delta \varphi) = N_2 \exp \left[-\frac{\left(\delta \varphi + \frac{\omega_r}{v_0^2} G \delta v \right)^2}{\sigma_\varphi^2} - \frac{\delta v^2}{\sigma_v^2} \right], \quad (\text{D9})$$

where $\delta \varphi = \varphi - \varphi_2$ and $\delta v = v - v_2$, with $\varphi_2 = \varphi_1 = \varphi_0 + (\omega_r/v_0)G$, $v_2 = v_1 + (E_0 L / m v_0)$. This means that the center velocity of the electron ensemble increases and there is no deformation in the shape of the ensemble, which is shown in Figs. 7(b2) and 7(b6). Thus, we call these units acceleration units. Similarly, when the ray passes through a prism, its position and wave vector change as

$$k_x = k_{0x} + K_p, \quad (\text{D10})$$

$$x = x_0. \quad (\text{D11})$$

Since all the light beams undergo the same change in k_x , the shape of the distribution function remains unchanged and the center point becomes $x_1 = x_0$, $v_1 = v_0 + K_p$, which is shown in Figs. 7(d2) and 7(d6). With the condition that $(\omega_r/v_0) - k_0 = 0$, $\varphi_n + \phi_0 = 2h\pi$, where the synchronicity condition is broken, electrons with less φ obtain more velocity. Thus, for an ensemble where the faster electron has accumulated less relative phase, it can be focused in the parameter space of velocity, as shown in Fig. 7(b4). Thus, we called these units, focus units. For the initial distribution $f_3(\delta v, \delta \varphi) = N_3 \exp[-(\delta \varphi + (\omega_r/v_0^2)2G\delta v)^2 / \sigma_\varphi^2 - (\delta v^2 / \sigma_v^2)]$, which means the ensemble propagated in the free space for the distance of $2G$ and passed through an acceleration unit, the possibility density function becomes

$$f_4(\delta v, \delta \varphi) = N_4 \exp \left\{ -\left[\frac{\left(1 - \frac{2\omega_r G E_0 L}{m v_0^3} \right)^2}{\sigma_\varphi^2} + \frac{E_0^2 L^2}{m^2 v_0^2} \right] \delta \varphi^2 - \left(\frac{1}{\sigma_v^2} + \frac{4\omega_r^2 G^2}{\sigma_\varphi^2 v_0^4} \right) \delta v^2 + 2 \left[\frac{2\omega_r G}{\sigma_\varphi^2 v_0^2} \left(1 - \frac{2\omega_r G E_0 L}{m v_0^3} \right) - \frac{E_0 L}{\sigma_v^2 m v_0} \right] \delta \varphi \delta v \right\}, \quad (\text{D12})$$

where $\delta \varphi = \varphi - \varphi_4$ and $\delta v = v - v_4$, with $\varphi_4 = \varphi_3 = \varphi_0 + 2(\omega_r/v_0)G$, $v_4 = v_3 = v_0 + (E_0 L / m v_0)$. When $\omega_r G_1 / \sigma_\varphi^2 v_0^2 [1 - (2\omega_r G E_0 L / m v_0^3)]^2 = E_0 L / \sigma_v^2 m v_0$, the possibility

density function becomes

$$f_4(\delta v, \delta \varphi) = N_4 \exp \left[- \left(1 - \frac{1}{1 + \frac{\sigma_\varphi^2 v_0^4}{\sigma_v^2 \omega_r^2 G^2}} \right) \frac{\delta \varphi^2}{\sigma_\varphi^2} - \left(\frac{1}{\sigma_v^2} + \frac{\omega_r^2 G^2}{\sigma_\varphi^2 v_0^4} \right) \delta v^2 \right], \quad (\text{D13})$$

which means we can realize the focus of electrons in the parameter space of velocity since the standard deviation of the velocity is compressed. As shown in Figs. 7(b4) and 7(b5), by choosing the parameters $\omega_r G_1 / \sigma_\varphi^2 v_0^2 [1 - (2\omega_r G E_0 L / m v_0^3)]^2 < E_0 L / \sigma_v^2 m v_0$, the distribution of electrons becomes that electrons with lower velocities often have smaller relative phases. With further evolution in the free space, electrons are focused in the parameter space of relative velocity.

When the ray passes through a lens, its position and wave vector are

$$k_x = k_{0x} - \frac{x_0}{f} (x - x_0), \quad (\text{D14})$$

$$x = x_0, \quad (\text{D15})$$

where f is the focal length, which takes a positive number for the convex lens and a negative number for the concave lens. This process is shown in Fig. 7(d4). Similarly, for rays propagating for a distribution of $g_3(\delta k_x, \delta x) = N_3 \exp[-(\delta x - (2G/k_{0z})\delta k_x)^2 / \sigma_x^2 - (\delta k_x^2 / \sigma_{k_x}^2)]$, which means that the rays propagate in the free space for a distance of $2G$, and pass through a prism, when they pass through a convex lens, the intensity distribution function becomes

$$g_4(\delta k_x, \delta x) = N_4 \exp \left\{ - \left[\frac{(1 - \frac{2Gk_{0x}}{fk_{0z}})^2}{\sigma_x^2} + \frac{k_{0x}^2}{\sigma_{k_x}^2 f^2} \right] \delta x^2 - \left(\frac{1}{\sigma_{k_x}^2} + \frac{4G^2}{\sigma_x^2 k_{0z}^2} \right) \delta k_x^2 - 2 \left[\frac{k_{0x}}{\sigma_{k_x}^2 f} \left(1 - \frac{2Gk_{0x}}{fk_{0z}} \right) - \frac{2G}{\sigma_x^2 k_{0z}} \right] \delta x \delta k_x \right\}, \quad (\text{D16})$$

where $\delta x = x - x_4$ and $\delta k_x = k_x - k_{4x}$, with $x_4 = x_3 = x_0 + (2Gk_{0x}/fk_{0z})$, $k_{4x} = k_{3x} = k_{0x} + K_p$. When $k_{0x}/\sigma_{k_x}^2 f > G/\sigma_x^2 k_{0z}$ and propagating in free space for a certain length, the rays are focused, as shown in Figs. 7(d4) and 7(d5). With the discussion above, the particle accelerator system can be directly mapped to a geometrical optics system, which means that the lens design and ray tracing will support the accelerator design.

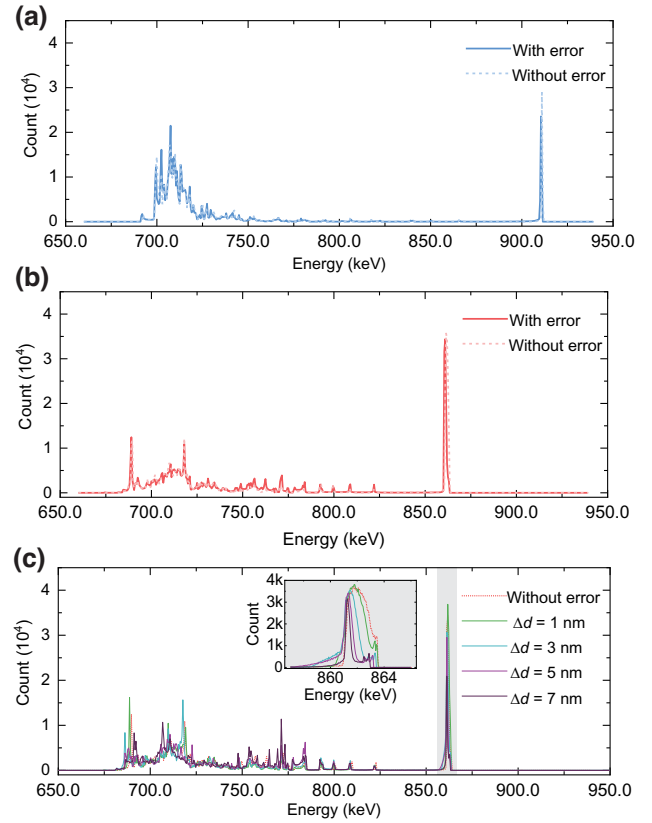


FIG. 8. The statistic of the final energy distribution for 500 000 input electrons, with the energy interval 0.5 keV. (a) For a target energy gain of 200 keV, the final energy distribution of electrons where no errors (blue dashed line) and 1-nm errors (blue solid line) are added to both the gap length and grating constant. (b) For a target energy gain of 150 keV, the final distribution of electrons where no errors (red dashed line) and 1-nm errors (red solid line) are added to both the gap length and grating constant. (c) When the target energy gain is 150 keV, the final distribution of electrons with no error (red dashed line) and 1-, 3-, 5-, and 7-nm errors (green, blue, purple, black solid lines) are added to the grating constant. Inset: enlarged distribution around the peak with an energy interval of 0.05 eV.

APPENDIX E: THE ROBUSTNESS OF THE MODULATION PROCESS

The robustness of the particle-acceleration process is useful because the control of the device parameters is not perfect in practice. For example, the device geometry parameters could not be precisely controlled due to limited nanofabrication precision. However, we expect the system to work properly when the errors (uncertainties) of the geometry parameters are at the nanometer scale, as allowed by current nanofabrication technology. Thus, an investigation of the relation between the uncertainty of parameters and acceleration efficiency is necessary. As discussed in the main text, the spatial-temporal modulation process can be optimized by controlling the grating constant and gap

length of each unit. As shown in Fig. 8, by adding errors to our optimized parameters (randomly plus or minus a certain number) for each unit, the final distribution of output is changed. According to our numerical simulations, with 1-nm errors in both the gap length and grating constant, the efficiency decreases by 26.7% when the target energy gain is 150 keV [Fig. 8(a)], while the efficiency is maintained when the target energy is 200 keV [Fig. 8(b)]. However, for the target energy gain of 200 keV, the linewidth of the spectrum is broadened when the errors are introduced.

Furthermore, the acceleration process can also be realized by controlling the grating constant and the phase of the input laser for each unit [6]. In addition, technologies to control the light phase are well developed, and a phase precision greater than 0.001π can be realized in our structure with current photonic technologies [47,48]. Thus, only the precision of the dielectric grating variation should be taken into consideration. If only the grating constant has errors due to the fabrication, for a target energy gain of 150 keV [Fig. 8(c)], the efficiency decreases by 0%, 23%, 46%, 71% for an introduced error of 1, 3, 5, 7 nm.

-
- [1] A. H. Atabaki, S. Moazeni, F. Pavanello, H. Gevorgyan, J. Notaros, L. Alloatti, M. T. Wade, C. Sun, S. A. Kruger, H. Meng, K. Al Qubaisi, I. Wang, B. Zhang, A. Khilo, C. V. Baiocco, M. A. Popović, V. M. Stojanović, and R. J. Ram, Integrating photonics with silicon nanoelectronics for the next generation of systems on a chip, *Nature* **556**, 349 (2018).
 - [2] Y. Meng, Y. Chen, L. Lu, Y. Ding, A. Cusano, J. A. Fan, Q. Hu, K. Wang, Z. Xie, Z. Liu, Y. Yang, Q. Liu, M. Gong, Q. Xiao, S. Sun, M. Zhang, X. Yuan, and X. Ni, Optical meta-waveguides for integrated photonics and beyond, *Light Sci. Appl.* **10**, 235 (2021).
 - [3] X. Qiang, X. Zhou, J. Wang, C. M. Wilkes, T. Loke, S. O’Gara, L. Kling, G. D. Marshall, R. Santagati, T. C. Ralph, J. B. Wang, J. L. O’Brien, M. G. Thompson, and J. C. F. Matthews, Large-scale silicon quantum photonics implementing arbitrary two-qubit processing, *Nat. Photonics* **12**, 534 (2018).
 - [4] Z. Zhao, S. Tan, K. Urbanek, T. Hughes, Y. J. Lee, S. Fan, J. S. Harris, and R. L. Byer, Silicon nitride waveguide as a power delivery component for dielectric laser accelerators, *Opt. Lett.* **44**, 335 (2019).
 - [5] T. W. Hughes, R. J. England, and S. Fan, Reconfigurable photonic circuit for controlled power delivery to laser-driven accelerators on a chip, *Phys. Rev. Appl.* **11**, 1 (2019).
 - [6] T. W. Hughes, S. Tan, Z. Zhao, N. V. Sapra, K. J. Leedle, H. Deng, Y. Miao, D. S. Black, O. Solgaard, J. S. Harris, J. Vuckovic, R. L. Byer, S. Fan, R. J. England, Y. J. Lee, and M. Qi, On-chip laser-power delivery system for dielectric laser accelerators, *Phys. Rev. Appl.* **9**, 54017 (2018).
 - [7] S. Tan, Z. Zhao, K. Urbanek, T. Hughes, Y. Lee, S. Fan, J. Harris, and R. Byer, Silicon nitride waveguide as a power delivery component for on-chip dielectric laser accelerators, *Opt. Lett.* **44**, 335 (2019).
 - [8] S. Jahani and Z. Jacob, All-dielectric metamaterials, *Nat. Nanotechnol.* **11**, 23 (2016).
 - [9] J. Hu, S. Bandyopadhyay, Y. H. Liu, and L. Y. Shao, A review on metasurface: From principle to smart metadevices, *Front. Phys.* **8**, 1 (2021).
 - [10] J. McNeur, M. Kozák, N. Schönenberger, K. J. Leedle, H. Deng, A. Ceballos, H. Hoogland, A. Ruehl, I. Hartl, R. Holzwarth, O. Solgaard, J. S. Harris, R. L. Byer, and P. Hommelhoff, Elements of a dielectric laser accelerator, *Optica* **5**, 687 (2018).
 - [11] N. V. Sapra, K. Y. Yang, D. Verduyck, K. J. Leedle, D. S. Black, R. J. England, L. Su, R. Trivedi, Y. Miao, O. Solgaard, R. L. Byer, and J. Vucković, On-chip integrated laser-driven particle accelerator, *Science* **367**, 79 (2020).
 - [12] R. Shiloh, J. Illmer, T. Chlouba, P. Yousefi, N. Schönenberger, U. Niedermayer, A. Mittelbach, and P. Hommelhoff, Electron phase-space control in photonic chip-based particle acceleration, *Nature* **597**, 498 (2021).
 - [13] Z. Chen, K. Koyama, M. Uesaka, M. Yoshida, and R. Zhang, Grating-based waveguides for dielectric laser acceleration, *Appl. Phys. Lett.* **113**, 124101 (2018).
 - [14] O. Kfir, H. Lourenço-Martins, G. Storeck, M. Sivis, T. R. Harvey, T. J. Kippenberg, A. Feist, and C. Ropers, Controlling free electrons with optical whispering-gallery modes, *Nature* **582**, 46 (2020).
 - [15] J.-W. Henke, A. S. Raja, A. Feist, G. Huang, G. Arend, Y. Yang, F. J. Kappert, R. N. Wang, M. Möller, J. Pan, J. Liu, O. Kfir, C. Ropers, and T. J. Kippenberg, Integrated photonics enables continuous-beam electron phase modulation, *Nature* **600**, 653 (2021).
 - [16] M. Kozák, Low-power light modifies electron microscopy, *Nature* **600**, 610 (2021).
 - [17] L. Fan, C.-L. Zou, N. Zhu, and H. X. Tang, Spectrotemporal shaping of itinerant photons via distributed nanomechanics, *Nat. Photonics* **13**, 323 (2019).
 - [18] A. Ashkin, Acceleration and trapping of particles by radiation pressure, *Phys. Rev. Lett.* **24**, 156 (1970).
 - [19] D. Leibfried, R. Blatt, C. Monroe, and D. Wineland, Quantum dynamics of single trapped ions, *Rev. Mod. Phys.* **75**, 281 (2003).
 - [20] C. Renaut, B. Cluzel, J. Dellinger, L. Lalouat, E. Picard, D. Peyrade, E. Hadji, and F. de Fornel, On chip shapeable optical tweezers, *Sci. Rep.* **3**, 2290 (2013).
 - [21] A. Ashkin, J. M. Dziedzic, J. E. Bjorkholm, and S. Chu, Observation of a single-beam gradient force optical trap for dielectric particles, *Opt. Lett.* **11**, 288 (1986).
 - [22] C. E. Wieman, D. E. Pritchard, and D. J. Wineland, Atom cooling, trapping, and quantum manipulation, *Rev. Mod. Phys.* **71**, S253 (1999).
 - [23] A. M. Kaufman, B. J. Lester, and C. A. Regal, Cooling a single atom in an optical tweezer to its quantum ground state, *Phys. Rev. X* **2**, 041014 (2012).
 - [24] J. Beugnon, C. Tuchendler, H. Marion, A. Gaëtan, Y. Miroshnychenko, Y. R. Sortais, A. M. Lance, M. P. Jones, G. Messin, A. Browaeys, and P. Grangier, Two-dimensional transport and transfer of a single atomic qubit in optical tweezers, *Nat. Phys.* **3**, 696 (2007).

- [25] J. Breuer and P. Hommelhoff, Laser-based acceleration of nonrelativistic electrons at a dielectric structure, *Phys. Rev. Lett.* **111**, 134803 (2013).
- [26] E. A. Peralta, K. Soong, R. J. England, E. R. Colby, Z. Wu, B. Montazeri, C. McGuinness, J. McNeur, K. J. Leedle, D. Walz, E. B. Sozer, B. Cowan, B. Schwartz, G. Travish, and R. L. Byer, Demonstration of electron acceleration in a laser-driven dielectric microstructure, *Nature* **503**, 91 (2013).
- [27] R. J. England, *et al.*, Dielectric laser accelerators, *Rev. Mod. Phys.* **86**, 1337 (2014).
- [28] C. Roques-Carnes, S. E. Kooi, Y. Yang, N. Rivera, P. D. Keathley, J. D. Joannopoulos, S. G. Johnson, I. Kaminer, K. K. Berggren, and M. Soljačić, Free-electron-light interactions in nanophotonics, e-prints [ArXiv:2208.02368v2](https://arxiv.org/abs/2208.02368v2) (2022).
- [29] Z. Zhao, D. S. Black, R. J. England, T. W. Hughes, Y. Miao, O. Solgaard, R. L. Byer, and S. Fan, Design of a multichannel photonic crystal dielectric laser accelerator, *Photonics Res.* **8**, 1586 (2020).
- [30] R. Shiloh, T. Chlouba, and P. Hommelhoff, Quantum-coherent light-electron interaction in a scanning electron microscope, *Phys. Rev. Lett.* **128**, 235301 (2022).
- [31] U. Niedermayer, T. Egenolf, O. B. Frankenheim, and P. Hommelhoff, Alternating-phase focusing for dielectric-laser acceleration, *Phys. Rev. Lett.* **121**, 214801 (2018).
- [32] A. Feist, K. E. Echternkamp, J. Schauss, S. V. Yalunin, S. Schäfer, and C. Ropers, Quantum coherent optical phase modulation in an ultrafast transmission electron microscope, *Nature* **521**, 200 (2015).
- [33] R. Dahan, S. Nehemia, M. Shentcis, O. Reinhardt, Y. Adiv, X. Shi, O. Be'er, M. H. Lynch, Y. Kurman, K. Wang, and I. Kaminer, Resonant phase-matching between a light wave and a free-electron wavefunction, *Nat. Phys.* **16**, 1123 (2020).
- [34] R. Dahan, A. Gorlach, U. Haeusler, A. Karnieli, O. Eyal, P. Yousefi, M. Segev, A. Arie, G. Eisenstein, P. Hommelhoff, and I. Kaminer, Imprinting the quantum statistics of photons on free electrons, *Science* **373**, 1324 (2021).
- [35] K. Wang, R. Dahan, M. Shentcis, Y. Kauffmann, A. B. Hayun, O. Reinhardt, S. Tsesses, and I. Kaminer, Coherent interaction between free electrons and a photonic cavity, *Nature* **582**, 50 (2020).
- [36] Y. Adiv, K. Wang, R. Dahan, P. Broaddus, Y. Miao, D. Black, K. Leedle, R. L. Byer, O. Solgaard, R. J. England, and I. Kaminer, Quantum nature of dielectric laser accelerators, *Phys. Rev. X* **11**, 041042 (2021).
- [37] B. Zhang, D. Ran, R. Ianculescu, A. Friedman, J. Scheuer, A. Yariv, and A. Gover, Quantum wave-particle duality in free-electron-bound-electron interaction, *Phys. Rev. Lett.* **126**, 244801 (2021).
- [38] G. Baranes, R. Ruimy, A. Gorlach, and I. Kaminer, Free electrons can induce entanglement between photons, *npj Quantum Inf.* **8**, 32 (2022).
- [39] R. W. Boyd, *Nonlinear Optics* (Academic Press, New York, 2008), p. 77.
- [40] T. Plettner, P. P. Lu, and R. L. Byer, Proposed few-optical cycle laser-driven particle accelerator structure, *Phys. Rev. Spec. Top.-Ac.* **9**, 111301 (2006).
- [41] L. Fan, C.-L. Zou, M. Poot, R. Cheng, X. Guo, X. Han, and H. X. Tang, Integrated optomechanical single-photon frequency shifter, *Nat. Photonics* **10**, 766 (2016).
- [42] S. Y. Lee, *Accelerator Physics* (World Scientific Publishing Company, Singapore, 2004), p. 229.
- [43] V. M. Pirozhenko, in *Proc. EPAC'08* (JACoW Publishing, Geneva, Switzerland), p. 2746, <https://jacow.org/e08/papers/WEPP098.pdf>.
- [44] A. Liu, J. Liu, W. Peng, X.-B. Xu, G.-J. Chen, X. Ren, Q. Wang, and C.-L. Zou, Multigrating design for integrated single-atom trapping, manipulation, and readout, *Phys. Rev. A* **105**, 053520 (2022).
- [45] M. Notomi, Manipulating light with strongly modulated photonic crystals, *Rep. Prog. Phys.* **73**, 096501 (2010).
- [46] M. M. M. A. Bahabad and H. C. Kapteyn, Quasi-phase-matching of momentum and energy in nonlinear optical processes, *Nat. Photonics* **4**, 570 (2010).
- [47] M. Poot and H. X. Tang, Broadband nanoelectromechanical phase shifting of light on a chip, *Appl. Phys. Lett.* **104**, 061101 (2014).
- [48] W. Cheng, Z. Mian, C. Xi, M. Bertrand, A. Shams-Ansari, S. Chandrasekhar, P. Winzer, and M. L. Car, Integrated lithium niobate electro-optic modulators operating at CMOS-compatible voltages, *Nature* **562**, 101 (2018).